Neurobiology of Disease 119 (2018) 41–52

Contents lists available at ScienceDirect

Neurobiology of Disease

journal homepage: www.elsevier.com/locate/ynbdi

Large-conductance Ca^{2+}-activated potassium channels are potently involved in the inverse neurovascular response to spreading depolarization

Ákos Menyhárt[a,1], Attila E. Farkas[b,1], Dániel P. Varga[a], Rita Frank[a], Réka Tóth[a], Armand R. Bálint[a], Péter Makra[a], Jens P. Dreier[c,d,e,f,g], Ferenc Bari[a], István A. Krizbai[b,h], Eszter Farkas[a,*]

[a] Department of Medical Physics and Informatics, Faculty of Medicine and Faculty of Science and Informatics, University of Szeged, Szeged, Hungary
[b] Physiology and Pathology of the Blood-Brain Barrier Research Group, Molecular Neurobiology Research Unit, Institute of Biophysics, Biological Research Centre, Hungarian Academy of Sciences, Szeged, Hungary
[c] Center for Stroke Research Berlin, Charite´ University Medicine Berlin, Berlin, Germany
[d] Department of Neurology, Charite´ University Medicine Berlin, Berlin, Germany
[e] Department of Experimental Neurology, Charite´ University Medicine Berlin, Berlin, Germany
[f] Bernstein Center for Computational Neuroscience Berlin, Berlin, Germany
[g] Einstein Center for Neurosciences Berlin, Berlin, Germany
[h] Institute of Life Sciences, Vasile Goldis Western University, Arad, Romania

ARTICLE INFO

Keywords:
Calcium channels
Cerebral arteriole
Cerebral blood flow
Potassium
Potassium channels
Neurovascular coupling
Paxilline
Spreading depression
Spreading ischemia
Vasoconstriction

ABSTRACT

Recurrent spreading depolarizations occur in the cerebral cortex from minutes up to weeks following acute brain injury. Clinical evidence suggests that the immediate reduction of cerebral blood flow in response to spreading depolarization importantly contributes to lesion progression as the wave propagates over vulnerable tissue zones, characterized by potassium concentration already elevated prior to the passage of spreading depolarization. Here we demonstrate with two-photon microscopy in anesthetized mice that initial vasoconstriction in response to SD triggered experimentally with 1 M KCl is coincident in space and time with the large extracellular accumulation of potassium, as shown with a potassium indicator fluorescent dye. Moreover, pharmacological manipulations in combination with the use of potassium-sensitive microelectrodes suggest that large-conductance Ca^{2+}-activated potassium (BK) channels and L-type voltage-gated calcium channels play significant roles in the marked initial vasoconstriction under elevated baseline potassium. We propose that potassium efflux through BK channels is a central component in the devastating neurovascular effects of spreading depolarizations in tissue at risk.

1. Introduction

Spreading depolarization (SD) is the generic term for all waves of abrupt, near-complete breakdown of the neuronal transmembrane ion gradients that cause cytotoxic edema and propagate at about 3 mm/min in cerebral gray matter. The SD continuum describes the spectrum from short-lasting SDs in metabolically intact tissue to SDs of intermediate duration to terminal SD in severely ischemic tissue (Dreier and Reiffurth, 2015; Hartings et al., 2017). Accordingly, SDs occur in neurological disorders such as the apparently harmless migraine aura, aneurysmal subarachnoid hemorrhage, traumatic brain injury, malignant hemispheric stroke, or circulatory arrest (Dreier et al., 2009; Farkas et al., 2010; Lauritzen et al., 2011; Hinzman et al., 2014; Woitzik et al., 2013; Dreier et al., 2018).

SD is associated with a cerebral blood flow (CBF) response consisting of distinct phases (Ayata and Lauritzen, 2015). The main

Abbreviations: aCSF, artificial cerebrospinal fluid; APG-2, Asante Potassium Green 2 (a K^+-sensitive fluorescent dye); BK channel, large-conductance Ca^{2+}-activated potassium channel; CBF, cerebral blood flow; DC potential, direct current potential; $[K^+]_e$, extracellular K^+ concentration; LFP, local field potential; rSD, recurrent spreading depolarization; SD, spreading depolarization; SD1, the first spreading depolarization in a train of events; VGCC, voltage-gated Ca^{2+} channel; VSMC, vascular smooth muscle cell

* Corresponding author at: Department of Medical Physics and Informatics, Faculty of Medicine, Faculty of Science and Informatics, University of Szeged, Korányi fasor 9, H-6720 Szeged, Hungary.
E-mail address: farkas.eszter.1@med.u-szeged.hu (E. Farkas).
[1] These authors contributed equally to this work.

https://doi.org/10.1016/j.nbd.2018.07.026
Received 18 May 2018; Received in revised form 3 July 2018; Accepted 23 July 2018
Available online 24 July 2018
0969-9961/

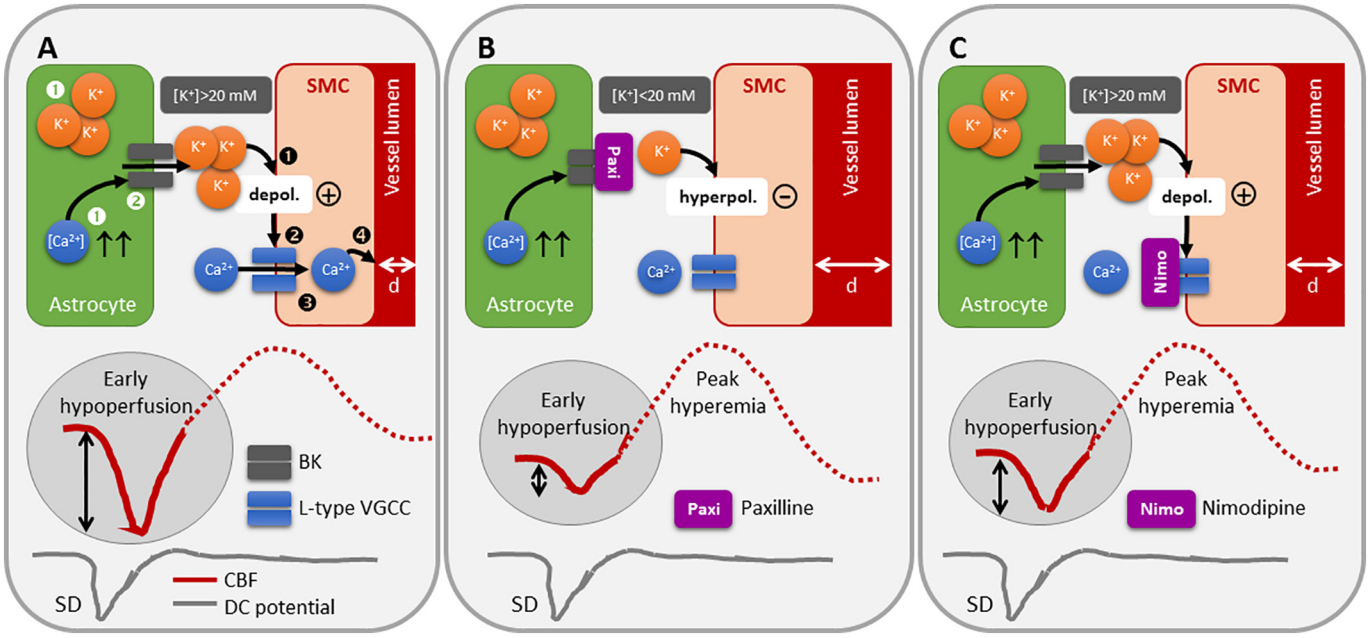

Fig. 1. Hypothesis driving the study, and pharmacological interventions utilized to prove the proposed concept. A, Spreading depolarization (SD; lowermost gray line) causes K^+ accumulation in the interstitium (Somjen, 2001; Pietrobon and Moskowitz, 2014); in turn, astrocytes take up surplus K^+ (Larsen and MacAulay, 2017), and a parallel rise of intracellular Ca^{2+} concentration occurs (Attwell et al., 2010; Li et al., 2012) (white ① in Astrocyte). The increased concentration of Ca^{2+} opens large-conductance Ca^{2+}-activated K^+ (BK) channels at the endfeet to allow K^+ efflux to the periarteriolar space (Girouard et al., 2010) (white ② in Astrocyte). Potassium accumulating at high concentration at the perivascular space (> 20 mM) drives the vascular smooth muscle cell (VSMC) membrane potential towards depolarization (Koide et al., 2012) (black ① in SMC). In turn, VSMC voltage-sensitive Ca^{2+} channels (VGCC) open (balck ② in VSMC) to give way to Ca^{2+} influx (black ③ in VSMC), which induces vasoconstriction (Koide et al., 2012) (black ④ in VSMC). This molecular signaling cascade is believed to underlie the initial hypoperfusion element of the cerebral blood flow (CBF) response to SD. B, Paxilline, a blocker of BK channels, is thought to be selective at the astrocyte endfeet given at concentrations below 1 μM (Girouard et al., 2010), and hinder the periarteriolar accumulation of K^+, thereby promoting hyperpolarization. As a result, VGCCs stay closed, and the vessel lumen is prone to be dilated. Paxilline administration, therefore, is expected to mitigate the early hypoperfusion element of the CBF response to SD. C, Nimodipine, a selective L-type VGCC blocker is applied to target VSMC channels (Alborch et al., 1995), K^+ current from astrocytes being presumably unaltered. As a direct consequence, Ca^{2+} influx is obstructed, vasoconstriction becomes hindered, and the initial hypoperfusion element of the CBF response to SD is anticipated to be smaller in magnitude.

hyperemic element of the CBF response is preceded by a short-lasting hypoperfusion especially discernible in the mouse brain (Fig. 1A). This early hypoperfusion has been identified as the most important parameter in the spectrum from normal hyperemic responses to inverse, vasoconstrictive responses, because it appears to override ensuing hyperemia in the ischemic cortex, thereby jeopardizing the survival of metabolically compromised tissue (Shin et al., 2006; Bere et al., 2014). Because ruling vasoconstriction (i.e. spreading ischemia) hampers the activation of energy-dependent membrane pumps such as the Na^+/K^+-ATPase, hence, the recovery from SD (Major et al., 2017), it prolongs the neuronal depolarization, the cytotoxic edema and the associated toxic intraneuronal Ca^{2+} and Na^+ surge. All these events together augment the risk of irreversible injury. Despite major clinical relevance, the mechanisms behind the CBF reduction in response to SD have not been fully elucidated (Dreier, 2011).

Under physiological conditions, astrocytes mediate vasodilation via Ca^{2+}-dependent activation of large conductance K^+ (BK) channels and K^+ release from astrocytic endfeet (Filosa et al., 2006). In turn, inward rectifier K^+ channels of vascular smooth muscle cells (VSMC) open, the VSMC membrane hyperpolarizes, and voltage-gated L-type Ca^{2+} channels (L-type VGCC) close, as long as the local rise in $[K^+]_e$ remains below 20 mM. Potassium triggers constriction of cerebral vessels at a concentration over 20 mM (Kuschinsky et al., 1972; Golding et al., 2000). SD is associated with a more than ten-fold elevation of $[K^+]_e$ from a baseline level of 3–4 mM to 30–60 mM (Vyskocil et al., 1972; Somjen, 1979), thus reaching the vasoconstrictive concentration range. From the beginning, K^+ has been a prime suspect to be involved in the initial constrictive element of the neurovascular response to SD (Dreier et al., 1998; Windmüller et al., 2005).Transition from astrocyte-evoked vasodilation to vasoconstriction occurs when the intra-astrocytic Ca^{2+} signal approximately doubles from normally 300–400 nM to 700–800 nM at the endfeet (Girouard et al., 2010). In this situation, BK channel activation is strongly enhanced, because the probability of BK channels to be open increases 16-fold when the cytoplasmic Ca^{2+} concentration doubles (Horrigan and Aldrich, 2002). As a consequence, local $[K^+]_e$ in the restricted perivascular space might exceed 20 mM. Under this condition, VSMCs depolarize, because the K^+ equilibrium potential declines, and L-type VGCCs open (Windmüller et al., 2005). Influx of Ca^{2+} then causes VSMCs to contract (Koide et al., 2012) (Fig. 1). Our main goal was to prove the key role of K^+ in the mediation of SD-related vasoconstriction, and to explore the involvement of BK channels and L-type VGCCs (Fig. 1).

It appears from previous investigations that the early vasoconstriction following SD may also be augmented if $[K^+]_e$ prior to or in between SD events is elevated over the physiological range (Dreier et al., 2000). Indeed, in experimental models of focal cerebral ischemia or subarachnoid hemorrhage, baseline $[K^+]_e$ was found to increase from 3 to 6–9 mM (Petzold et al., 2005; Hansen, 1977; Hansen and Zeuthen, 1981). In addition to predisposing the vessels to constrict in response to SD, higher baseline $[K^+]_e$ also predicted longer SD duration in brain slices, unrelated to vascular tone (Dreier et al., 2001). These experimental data have prompted us to analyze how the kinetics of K^+ accumulation with SD may be related to baseline $[K^+]_e$ prior to SD occurrence.

Changes in $[K^+]_e$ have been traditionally acquired with K^+-selective microelectrodes (Vyskocil et al., 1972; Hansen and Zeuthen, 1981), which lack spatiotemporal resolution necessary to establish coupling with CBF accurately. Recently, a novel K^+-sensitive fluorescent dye,

Asante Potassium Green 2 (APG-2; TEFLabs, Inc., Austin, TX, USA) has been applied successfully for the spatiotemporal monitoring of $[K^+]_e$ changes during ictal activity (Bazzigaluppi et al., 2015).

With the necessary tools now available, we set out to image SD-related changes in $[K^+]_e$ in association with rhodamine-dextran loaded cortical blood vessels using two-photon microscopy in mice. In other experiments, laser-Doppler flowmetry in combination with the use of K^+-sensitive microelectrodes aided the quantitative evaluation of $[K^+]_e$ and CBF. In this set of experiments, we also aimed to contemplate on the impact of baseline $[K^+]_e$ gradually increasing into the pathophysiological range (i.e. over 2–4 mM) on the kinetics of arising SD events. Finally, pharmacological inhibition of BK channels or L-type VGCCs revealed their contribution to the SD-induced initial vasoconstriction under elevated baseline $[K^+]_e$ (Fig. 1).

2. Materials and methods

The experimental procedures were approved by the National Food Chain Safety and Animal Health Directorate of Csongrád County, Hungary, conforming to the guidelines of the Scientific Committee of Animal Experimentation of the Hungarian Academy of Sciences (updated Law and Regulations on Animal Protection: 40/2013. (II. 14.) Gov. of Hungary), following the EU Directive 2010/63/EU on the protection of animals used for scientific purposes, and reported in compliance with the ARRIVE guidelines.

Anesthetized, adult, male C57Bl/6 mice ($n = 23$) were used for the study. Standard rodent chow and tap water were supplied ad libitum. The animals were housed under constant temperature, humidity, and lighting conditions (23 °C, 12:12 h light/dark cycle, lights on at 7 a.m.). There was no specific criterion formulated for inclusion or exclusion.

2.1. Two-photon microscopy

Mice ($n = 8$) were anesthetized with 1% Avertin (20 µl/g, i.p.), and mounted on a stereotactic frame incorporating a heating pad. A cranial window (d = 3 mm) was prepared on the right parietal bone, and the dura was retracted. The exposed brain surface was loaded with APG-2 dissolved in Ringer-HEPES solution (150 mM NaCl, 5.2 mM KCl, 2.2 mM $CaCl_2$, 0.2 mM $MgCl_2$, 6 mM $NaHCO_3$, 5 mM HEPES, 2.8 mM D-Glucose, pH = 7.4) to a concentration of 0.76 mM ($n = 7$) (TEFLabs, Inc., Austin, TX, USA) (Bazzigaluppi et al., 2015), or Ringer-HEPES solution as negative control for APG-2 ($n = 1$). The craniotomy was then coverslipped with a microscopic cover glass. A second, smaller trepanation was drilled rostral to the first craniotomy, to be used for SD elicitation (Fig. 2A). A glass capillary connected to a syringe pump (CMA/100, CMA/Microdialysis, Solna, Sweden) was filled with 1 M KCl, and was fastened to the skull with acrylic dental cement, with its tip positioned at the cortical surface within the rostral trepanation. Blood vessels were then loaded with 2–10 mg rhodamine-dextran (D1841, Life Technologies Magyarország Kft. Budapest, Hungary) in 100 µl Ringer-HEPES by retro-orbital injection.

In vivo intracranial microscopy was performed with a FEMTO2D-Alba microscope (Femtonics Ltd., Budapest, Hungary) using a 20× large working distance water objective (XLUMPLFLN-20XW, Olympus) using MES software (v4.6.2336, Femtonics). Two-photon excitation was performed using a Mai Tai HP Ti-sapphire laser (RK TECH Ltd., Budapest, Hungary) at 810 nm, which was found optimal for APG-2 excitation, and also adequate for rhodamine. Emission was detected with gallium arsenide phosphide photomultipliers, equipped with the appropriate color filters. Laser power was set to 10–40% depending on the depth of imaging (0–300 µm from the brain surface), photomultiplier voltages were set to 70%. A z-stack with 5 µm vertical steps was recorded at the area of interest for identification of arterioles and venules, then image sequences were taken of the desired vessel cross sections at approximately 1 µm/pixel spatial and 0.8–2 Hz temporal resolution.

After acquiring baseline images, SD was triggered repeatedly at intervals of 15–20 min in the rostral cranial window by the ejection of 1–4 µl 1 M KCl to the brain surface through the glass capillary. Image sequences of APG-2 and rhodamine dextran were captured continuously for 10 min. Image stacks were auto leveled, merged and converted to RGB color in FIJI (Schindelin et al., 2012) for manual vessel diameter measurements.

2.2. Electrophysiology and cerebral blood flow assessment

Mice ($n = 15$) were anesthetized with 1.5–2% isoflurane in N_2O:O_2 (2:1), and body temperature was maintained at 37 °C using a heating pad (Harvard Apparatus, Holliston, MA, USA). Once the animal was placed in a stereotactic frame, two adjacent craniotomies were opened on the right parietal bone, with the dura left intact. The rostral window was used for SD elicitation, while a K^+-sensitive microelectrode and a laser-Doppler flowmetry probe were placed in the caudal window.

Ion-sensitive microelectrodes were prepared according to Viitanen et al. (2010). Glass capillary microelectrode tips (outer diameter: 10–12 µm) were filled with a liquid K^+-ion exchanger (Potassium ionophore I - cocktail A; Sigma) (Bazzigaluppi et al., 2015), and the shank of the microelectrode was backfilled with 100 mM KCl. Each K^+-sensitive microelectrode was calibrated in standard solutions of known K^+ concentrations (1, 3, 5, 10, 30, 50, 100 mM). In each experiment, a K^+-sensitive microelectrode was lowered into the cortex, together with another microelectrode (tip diameter = 20 µm) filled with 150 mM NaCl and 1 mM HEPES to serve as reference. The reference electrode acquired local field potential (LFP) filtered in direct current (DC) potential mode. An Ag/AgCl electrode implanted under the skin of the animal's neck was used as common ground. Microelectrodes were connected to a custom-made dual-channel high input impedance electrometer (including AD549LH, Analog Devices, Norwood, MA, USA) via Ag/AgCl leads. The voltage signal recorded by the reference electrode was subtracted from that of the K^+-sensitive microelectrode by dedicated differential amplifiers and associated filter modules (NL106 and NL125, NeuroLog System, Digitimer Ltd., United Kingdom), which yielded potential variations related to changes in $[K^+]_e$. The recorded signals were then forwarded to an analog-to-digital converter (MP 150, Biopac Systems, Inc). Electric signals were continuously acquired at a sampling frequency of 1 kHz. Changes of $[K^+]_e$ were expressed in mV to be translated into mM concentration offline, using least squares linear regression.

CBF variations were monitored with a laser-Doppler needle probe (Probe 403 connected to PeriFlux 5000; Perimed AB, Sweden) positioned at an angle next to the penetration site of the K^+-sensitive microelectrode. The flow signal was digitized and displayed together with the DC potential and K^+ signals as described above (MP 150 and AcqKnowledge 4.2.0, Biopac Systems, Inc. USA). The completed preparations were enclosed in a Faraday cage.

2.3. Pharmacological treatments and elicitation of SD

Paxilline (a BK channel inhibitor), dissolved in artificial cerebrospinal fluid (aCSF; 500 nM; $n = 6$; composition of aCSF in mM concentrations: 126.6 NaCl, 3 KCl, 1.5 $CaCl_2$, 1.2 MgCl, 24.5 $NaHCO_3$, 6.7 urea, 3.7 glucose bubbled with 95% O_2 and 5% CO_2 to achieve a constant pH of 7.4) or nimodipine (L-type VGCC blocker, dissolved in 0.1% DMSO, 100 µM; $n = 5$) (Richter et al., 2002) were administered topically in the caudal cranial window after the initiation of 2–3 SDs at a 15 min interval. Animal selection for treatment was random by alternating treatment as the experimental work proceeded. Four subsequent SDs, 15 min apart, were elicited following 20 min incubation in drug solutions. Drug solutions were regularly refreshed (i.e. every 10 min) until the termination of each experiment. The concentration of paxilline was chosen with the guidance of a previous report (Girouard et al., 2010) and refined on the basis of our own pilot experiments

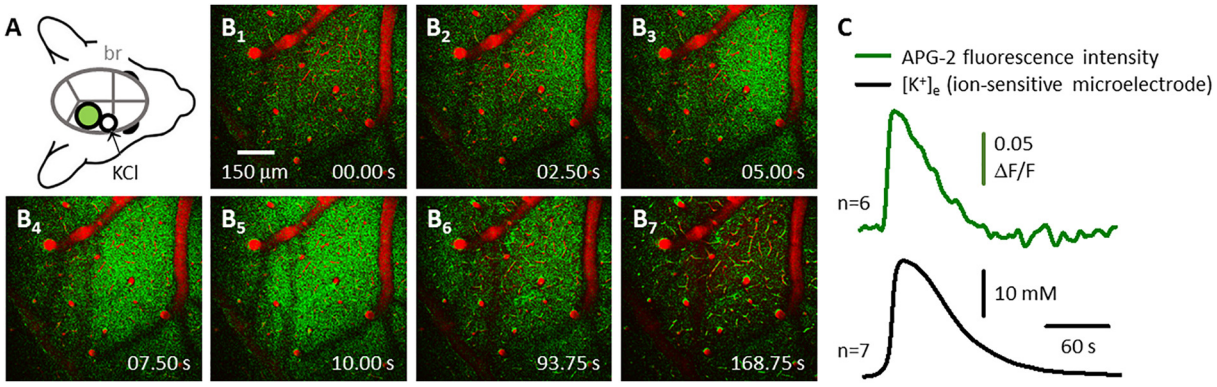

Fig. 2. APG-2 fluorescence intensity corresponds with variations in the extracellular concentration of potassium ($[K^+]_e$) during spreading depolarization (SD) over the mouse parietal cortex. A, Schematic illustration shows the position of the cranial window (green) used for image acquisition, to aid the orientation of images in Panels $B_{1–7}$. SD events were triggered by KCl through a smaller craniotomy (open circle) frontal to the site of imaging and caudal to bregma (br). $B_{1–7}$, Pseudo-colored, contrast-enhanced, two-photon microscopic images demonstrate the progressive elevation of APG-2 fluorescence intensity (green) with the propagation of an SD (from fronto-medial to caudo-lateral direction). Optical APG-2 signal was intensified in the images by background subtraction over the green channel. The vascular architecture is delineated by intravascular rhodamine dextran (red). Images were taken at a cortical depth of 50–55 µm. C, Measurement of $[K^+]_e$ with ion-sensitive glass microelectrodes (black trace, mean of 7 SD events) confirms that the kinetics of APG-2 fluorescence intensity extracted from a single region of interest (green trace, mean of 6 SD events) indicates SD-related changes in $[K^+]_e$. (For interpretation of the references to color in this figure legend, the reader is referred to the web version of this article.)

utilizing 100, 500 nM and 1 µM concentration paxilline solutions (data not shown). Control experiments ($n = 4$) were carried out by rinsing the caudal cranial window with aCSF throughout the experimental protocol. In addition, recurrent SDs triggered before drug administration in the paxilline and nimodipine groups were also taken as control.

SDs were elicited in the rostral craniotomy by placing a cotton ball soaked in 1 M KCl on the cortical surface, and removing it after the detection of each SD. In some cases ($n = 4$), the cotton ball was left in the cranial window, to achieve a gradual elevation of baseline K^+ concentration at the site of data acquisition. This approach progressively elevated K^+ levels to reproduce conditions typical of injured tissue, and enabled the assessment of the interaction between baseline $[K^+]_e$, the kinetics of SD events, and the associated CBF response.

2.4. Application of paxilline to acute, live neocortical brain slices

Male, adult Sprague Dawley rats (body weight: 250 g; $n = 11$) were decapitated under deep anesthesia (4–5% isoflurane in N_2O:O_2; 2:1). Brain slices were obtained following a previously established protocol (Kocsis et al., 2016). Briefly, coronal brain slices (350 µm) anterior to bregma were cut with a vibrating blade microtome (Leica VT1000S), and collected in ice-cold aCSF (composition of aCSF in mM concentrations: 130 NaCl, 3.5 KCl, 1 NaH_2PO_4, 24 $NaHCO_3$, 1 $CaCl_2$, 3 $MgSO_4$ and 10 D-glucose). Six to eight slices were transferred to an incubation chamber filled with carbogenated aCSF (difference in composition in mM concentrations: 3 $CaCl_2$ and 1.5 $MgSO_4$), and kept at room temperature (~20 °C). Selected slices were placed into an interface type recording tissue chamber (Brain Slice Chamber BSC1, Scientific Systems Design Inc., Ontario, Canada) continuously perfused with carbogenated aCSF at a rate of 2 ml/min, and kept at 32 °C using a dedicated proportional temperature controller unit (PTC03, Scientific Systems Design Inc., Ontario, Canada).

For LFP recording, a glass capillary electrode (20 µm outside tip diameter) filled with 150 mM NaCl and 1 mM HEPES was inserted into layers 3–4 of the cerebral cortex, the bottom of the tissue chamber containing an Ag/AgCl reference electrode. LFP was recorded via a custom-made dual-channel high input impedance electrometer (including AD549LH, Analog Devices, Norwood, MA, USA), connected to a differential amplifier (NL106, NeuroLog System, Digitimer Ltd., United Kingdom) with associated filter and conditioner systems (NL125, NL530, NeuroLog System, Digitimer Ltd., United Kingdom). Potential line frequency noise (50 Hz) was removed by a high quality noise eliminator (HumBug, Quest Scientific Instruments Inc., Canada) without any signal attenuation. The resulting signal was digitalized by an analog/digital (A/D) converter (MP150, Biopac Systems Inc., USA) and continuously acquired at a sampling frequency of 1 kHz using the software AcqKnowledge 4.2.0 (Biopac Systems Inc., USA).

SDs were triggered by electric stimulation as reported earlier (Hertelendy et al., 2017). A concentric bipolar needle electrode (tip size: 40 µm, Neuronelektród Kft., Hungary) was placed at a distance of approximately 800–1000 µm from the recording electrode. The stimulating electrode was connected to an opto-coupled stimulus isolator with constant current output (NL 800, Digitimer Ltd., United Kingdom) a pulse generator (NL301), a with-delay panel (NL405) and a pulse buffer (NL510), which enabled the adjustment of the duration of the stimuli at will. Stimulation was implemented with single, cathodal constant current pulses. The charge delivered to achieve successful SD elicitation ranged from 50 to 1500 µC. Four to six SDs were triggered in each slice, at an interval of 12 min. The stimulating electrode was repositioned prior to each SD, to optimize contact between the electrode tip and viable tissue.

In control experiments (brain slices: $n = 4$, SDs analyzed: $n = 20$), brain slices were kept in carbogenated aCSF throughout the experimental protocol. For paxilline treatment, various concentrations of the drug (dissolved in aCSF) were tested (100 nM: brain slices: n = 2 SDs analyzed: $n = 10$; 250 nM: brain slices: n = 2 SDs analyzed: $n = 12$; 500 nM: brain slices: $n = 5$ SDs analyzed: n = 20) to select the lowest effective dose. The first SD (SD1) in a train was triggered under aCSF to serve as reference in each slice. Subsequent, recurrent SDs (rSD) were elicited after paxilline administration.

2.5. Data processing and analysis

The optical signal of APG-2 was analyzed with a dedicated macro written in the software ImagePro Plus (Media Cybernetics, Rockville, MD, USA). Local changes in APG-2 fluorescence intensity with time were extracted by placing regions of interest (ROIs) of 15 × 15 µm size (corresponding to the tip size of K^+-sensitive microelectrodes) at selected parenchymal locations in the image sequences.

Vascular lumen diameter changes were measured in the software ImageJ (National Institute of Health, Bethesda, USA). Vascular changes related to SD1 were analyzed apart from subsequent, rSD events. Pial arterioles, penetrating arterioles and cortical venules were identified with the help of 3D reconstruction relying on a z-stack of two-photon

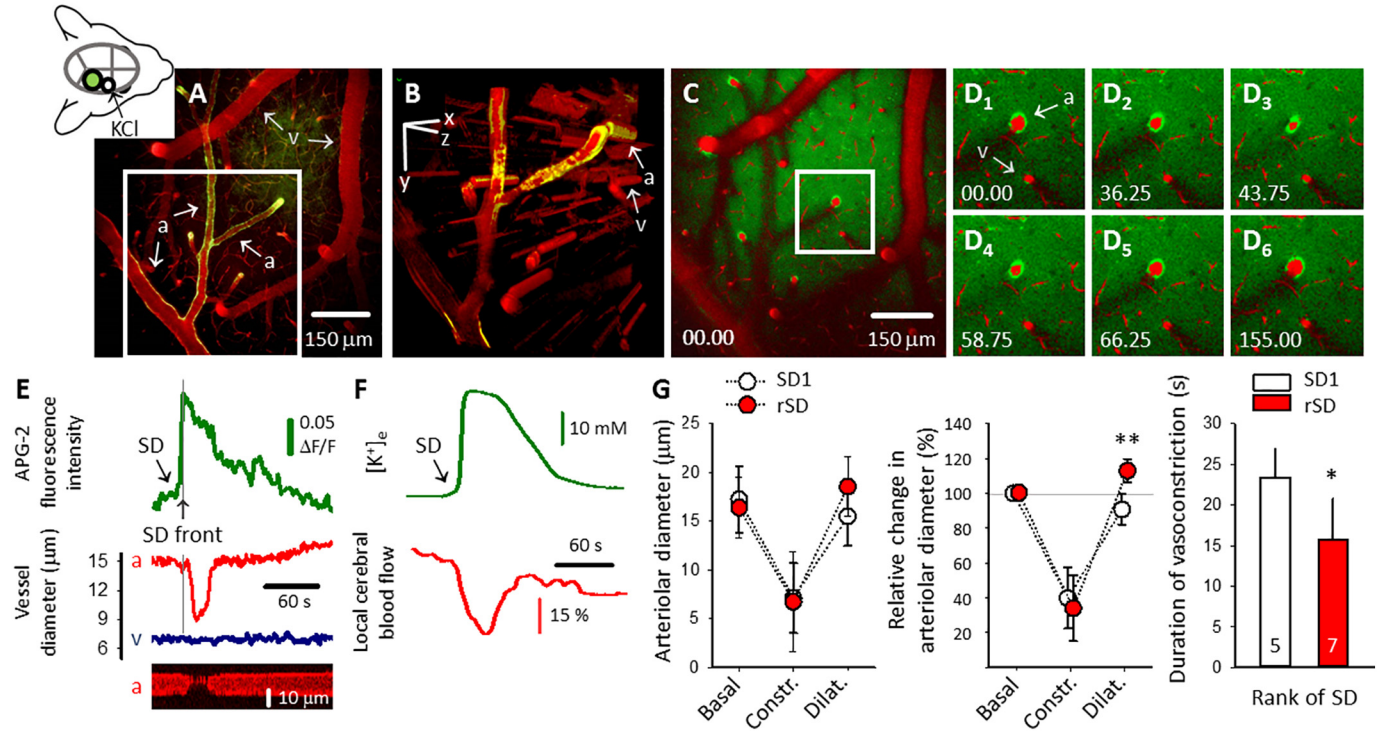

Fig. 3. A marked transient increase in the extracellular concentration of potassium ($[K^+]_e$) with the first spreading depolarization in a train (SD1) is coincident with vasoconstriction of penetrating arterioles at the SD wave-front, and a brief drop of local cerebral blood flow (CBF), in the mouse parietal cortex. A, Schematic illustration of the preparation in the upper left hand corner is provided for the orientation of images in Panels A-D. The cranial window used for image acquisition is colored green. The full image presents a representative *Z*-projection of 130 images taken over a cortical depth of 200 µm. Blood vessels were loaded with rhodamine dextran (red), and are delineated by traces of APG-2 (green/yellow). Arrows labeled with "a" designate arterioles, "v" labels venules. Note, that venules are devoid of any APG-2 contour. The white frame outlines the area reconstructed in Panel B. B, Three-dimensional z-stack reconstruction of the microvascular architecture in the cortical volume (depth = 200 µm) scanned by two-photon microscopy, which allows the identification of vessel types. The arrow with "a" is pointing at a penetrating arteriole and "v" indicates an adjacent venule, both shown in cross section in Panels C & $D_{1–6}$. C, A pseudo-colored, contrast enhanced, representative, single snap shot taken at a cortical depth of 50–55 µm is the first image in a series used for the measurement of changes in vessel diameters. APG-2 loaded in the tissue is green; red labels rhodamine dextran in vessels. The white frame indicates the area shown in Panels $D_{1–6}$. $D_{1–6}$, Series of images demonstrates constriction of a cortical penetrating arteriole in response to SD1; the cross section of the tiny venule remains unaltered. E, Red trace and kymograph below depict SD1-associated diameter changes of a penetrating arteriole, and blue trace stands for an irresponsive venule, both presented in Panels $D_{1–6}$; Green trace shows the corresponding variation in APG-2 fluorescence indicative of $[K^+]_e$, derived from the same images. The kymograph was created in FIJI by correcting the image stack for drift using the Template Matching plugin (Hsu et al., 2012) followed by the KymographBuilder plugin (DOI https://doi.org/10.5281/zenodo.591877) on a line drawn along the diameter of the vessel. F, Representative traces demonstrate a typical $[K^+]_e$ shift and the associated drop of CBF to SD1, recorded with an intracortical potassium-sensitive microelectrode and laser-Doppler flowmetry in a separate mouse. Note a good correspondence with the signals presented in Panel E. G, Absolute and relative changes of penetrating arteriolar diameter, and duration of vasoconstriction in response to SD1, and recurrent SD (rSD) events. Data are given as mean ± stdev; $n = 12$. Sample size (i.e. number of vessels analyzed) is indicated in each bar. One-way analysis of variance (ANOVA) was used for statistical analysis; the level of significance is given as p* < 0.05 and p** < 0.01. (For interpretation of the references to color in this figure legend, the reader is referred to the web version of this article.)

images of intravascular rhodamine dextran-loaded tissue (Fig. 3A–B). 3D images were constructed using the built-in 3D viewer in ImageJ 1.5i with Java 1.6.0_24 (64 bit). Either cross sections (typically penetrating arterioles or parenchymal venules) or longitudinal sections (pial arterioles) in the focal plane of the recorded videos were selected for the measurement of vascular lumen diameter changes. The criteria to include a vessel into the analysis were the following: the potassium wave of SD must have propagated fully over the parenchyma next to the vessel; The baseline diameter of penetrating arterioles was above 10 µM in order to have reliable assessment of vasoconstriction with respect to pixel size (i.e. 1 µm); the penetrating arteriole was a first order arteriole branching from a pial arteriole; the penetrating vessel optimally appeared in cross sectional view. Three, independent investigators ran the diameter analysis for each selected vessel, and the three data sets were averaged.

Quantitative data are given as mean ± standard deviation (stdev). Statistical analysis was conducted with the software SPSS (IBM SPSS Statistics for Windows, Version 22.0, IBM Corp.). Data sets were evaluated by either a one-way analysis of variance (ANOVA) followed by a Fisher post hoc test, or a Pearson one-tailed correlation analysis model. Level of significance was set at $p < .05$* or $p < .01$**. Appropriate statistical methods are provided in each Figure legend in detail.

3. Results

3.1. Imaging the $[K^+]_e$ wave of SD with two-photon microscopy

The fluorescence intensity of APG-2 sharply increased with each SD triggered (amplitude: 0.14 ± 0.03 ΔF/F, peak corresponding to $[K^+]_e$ of 35.5 ± 5.3 mM measured in the electrophysiology series of experiments) (Fig. 2). The increased fluorescent signal propagated across the field of view at a rate of 3.36 ± 1.67 mm/min, typical of SD. In the absence of APG-2, but under otherwise identical experimental conditions (control experiment), SD occurrence was confirmed by typical cerebrocortical vascular reactions, but no optical signal of SD was captured. These observations validate that the optical signal acquired in the APG-2 experiments was specific to the dye (Bazzigaluppi et al., 2015). The APG-2 signature of SD lasted shorter than the $[K^+]_e$ shift recorded with ion-sensitive microelectrodes (29.8 ± 9.0 vs. 57.7.1 ± 17.8 s, respectively), but varied clearly within the same order

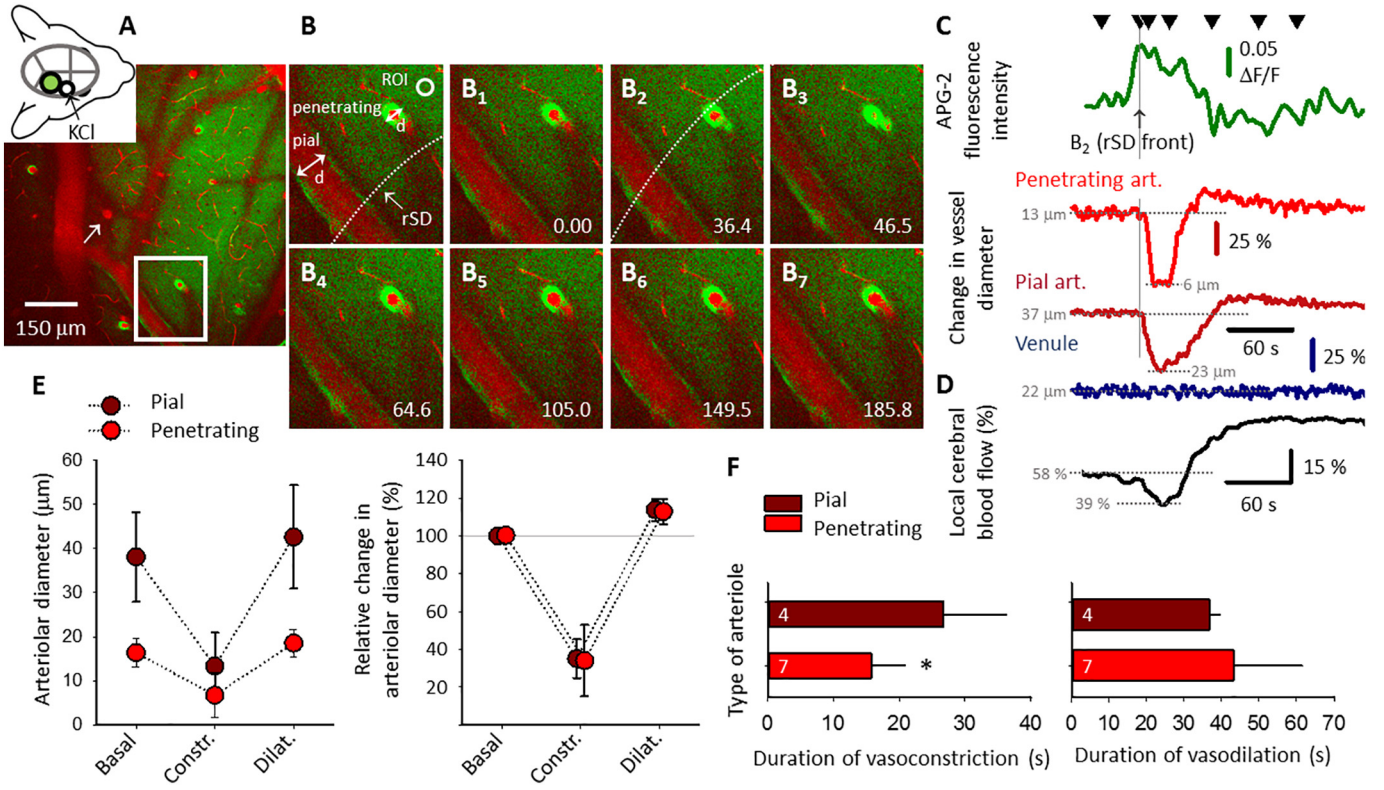

Fig. 4. Both pial and penetrating arteriolar constriction are spatiotemporally synchronous with the elevation of the extracellular concentration of potassium ($[K^+]_e$) with recurrent spreading depolarization (rSD). A, Schematic illustration of the preparation in the upper left hand corner is given for the orientation of images in Panels B. The cranial window used for image acquisition is colored green. A pseudo-colored, contrast enhanced, representative, single snap shot taken at a cortical depth of 50–55 µm shows the field of view. APG-2 loaded in the tissue is green; red designates rhodamine dextran in vessels. The white frame outlines the area shown in Panels B; white arrow labels a venule analyzed for Panel C. B, The positions of diameter measurement (d) of a pial arteriole in longitudinal view and a penetrating arteriole in cross sectional view are aligned with a region of interest (ROI) used for the extraction of APG-2 fluorescence intensity. All three measurement positions are arranged along the front of an rSD wave to examine synchronicity between increasing APG-2 fluorescence and arteriolar response. $B_{1–7}$, Images illustrate diameter changes of the selected pial and penetrating arterioles in response to rSD. Note the initial constriction in $B_{1–3}$, and the subsequent dilation in $B_{4–7}$. C, The green trace representing APG-2 fluorescence variation with rSD was acquired at the ROI shown in Panel B. Red traces illustrate the coupled arteriolar responses, while the blue trace tracks diameter changes of the venule indicated by an arrow in Panel A. Black triangles above the traces give the sampling time of the images in Panels $B_{1–7}$. Note, that the peak intensity of APG-2 fluorescence coincides with the onset of arteriolar constriction. D, A representative trace illustrates the local cerebral blood flow response to an rSD event, acquired with laser-Doppler flowmetry over the parietal cortex of another mouse. Note a good correspondence to the reactions of arterioles presented in Panel C. E, Absolute and relative changes of pial and penetrating arteriolar diameter in response to rSD. Data are given as mean ± stdev. F, Duration of vasoconstriction and vasodilation in response to rSD. Data are given as mean ± stdev; $n = 11$. Sample size (i.e. number of vessels analyzed) is indicated in each bar. One-way analysis of variance (ANOVA) was used for statistical analysis; the level of significance is given as $p^* < 0.05$. (For interpretation of the references to color in this figure legend, the reader is referred to the web version of this article.)

of magnitude (Fig. 2C). In conclusion, features of the APG-2 fluorescent signal of SD convincingly suggest, that APG-2 indicates SD-related changes in $[K^+]_e$ (Fig. 2).

3.2. Vascular response to spreading depolarization in the mouse cortex

Vascular reaction to SD concerned arterioles only, which displayed a robust constriction (Fig. 3A–E); venules did not undergo diameter adjustment (Fig. 3E & 4C). Penetrating arterioles were taken for the comparison of vascular reactions to SD1 and rSD events. SD1 induced marked, transient arteriolar constriction alone (from 17.2 ± 3.4 to 7.1 ± 3.6 µm) (Fig. 3G). Subsequent rSDs caused an initial, short, marked constriction of arterioles (from 16.4 ± 3.2 to 6.7 ± 5.1 µm), followed by longer-lasting vasodilation (to 18.5 ± 3.2 µm, duration: 43.1 ± 18.3 s) (Fig. 3G). The degree of vasoconstriction was similar but its duration was significantly shorter-lasting for rSDs than for SD1 (15.7 ± 5.1 vs. 23.4 ± 3.5 s) (Fig. 3G). The observed changes in arteriolar caliber were consistent with the kinetics of SD-related CBF variations assessed with laser-Doppler flowmetry in other mice (for SD1: Fig. 3E–F, for rSDs: Fig. 4C–D). Overall, CBF transiently dropped from 100.0 ± 0.8 to 74.0 ± 9.1% in response to SD1, and from 60.4 ± 5.1 to 47.4 ± 11.7% in response to rSDs. The subsequent hyperemic element of the CBF response to rSDs peaked at 77.9 ± 8.1% and persisted for 99.1 ± 61.7 s.

The baseline lumen diameter before rSDs was apparently narrower for penetrating than for pial arterioles (16.4 ± 3.2 vs. 38.1 ± 10.2 µm), but their SD-related, maximal constriction relative to baseline tone was essentially identical (34.0 ± 18.8 vs. 35.1 ± 10.3%) (Fig. 4E). Likewise, penetrating and pial arterioles later dilated in response to rSD to an equal degree (113.0 ± 6.8 vs. 113.8 ± 5.8%), which persisted for a similar duration (43.1 ± 18.3 vs. 36.8 ± 2.9 s) (Fig. 4F). The duration of initial vasoconstriction proved to be shorter for penetrating as compared with pial arterioles (15.7 ± 5.1 vs. 26.8 ± 9.4 s) (Fig. 4F), consistent with the more rapid progress of vasoconstriction in penetrating arterioles (i.e. maximal vasoconstriction in pial arterioles was achieved with a delay of 3.31 ± 1.3 s with respect to penetrating arterioles).

3.3. Synchronicity of high $[K^+]_e$ and constriction of cortical arterioles in response to SD

Constriction of both pial and penetrating arterioles was in tight

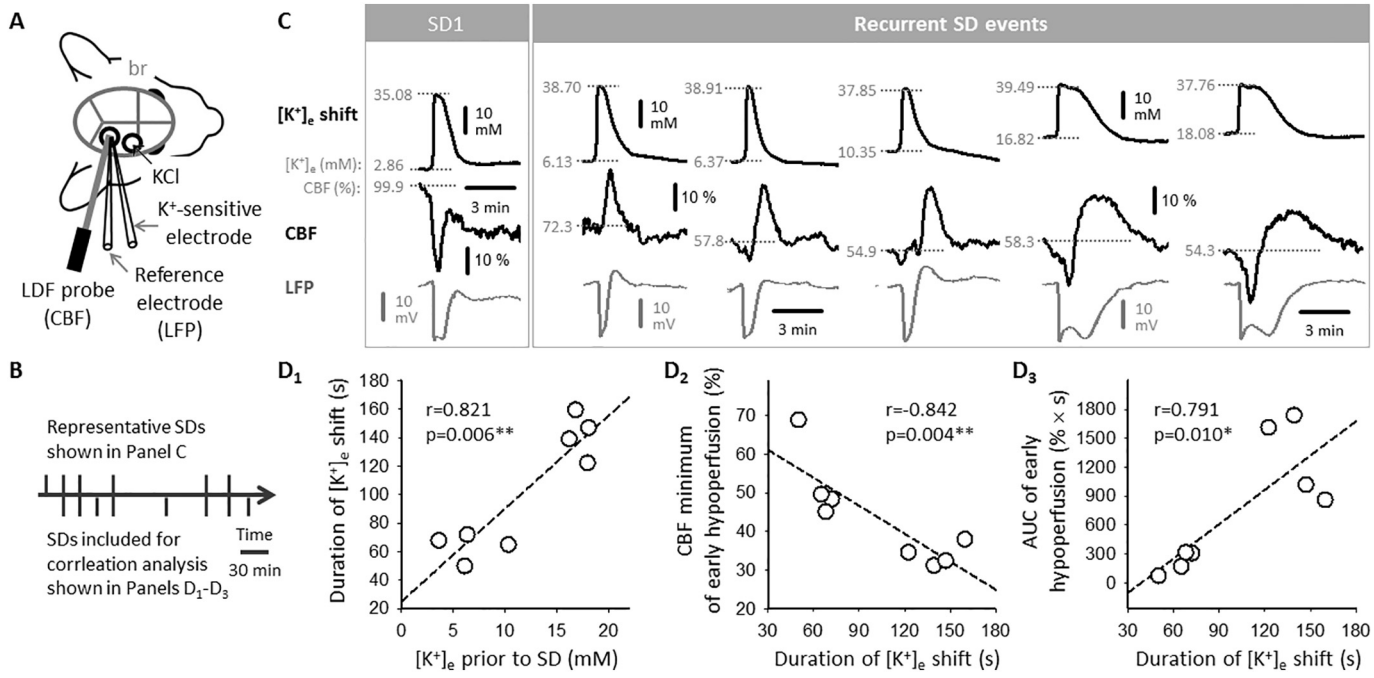

Fig. 5. Association between extracellular potassium concentration ($[K^+]_e$) and the prominence of early hypoperfusion in response to recurrent spreading depolarization (SD) in the mouse cerebral cortex. A, Experimental preparation for conventional electrophysiological data acquisition. The caudal cranial window served as recording site, and the rostral window was used for SD elicitation by the topical application of 1 M KCl. B, Time line of a representative experiment indicates SD events (vertical stripes) used for detailed analysis presented in Panels C and $D_{1–3}$. C, Recurrent SD events (rSD; gray traces), the associated variation of $[K^+]_e$ (black traces) and the coupled cerebral blood flow (CBF) response transformed as a function of increasing baseline $[K^+]_e$ (initial segment of black traces). D, Correlation analysis between baseline $[K^+]_e$ and the duration of the transient rise of $[K^+]_e$ with rSDs (D_1), the duration of the transient rise of $[K^+]_e$ and the minimum value of the early hypoperfusion element of the CBF response to rSD (D_2), and the duration of the transient rise of $[K^+]_e$ and the area under the curve (AUC) of early hypoperfusion (D_3). A Pearson one-tailed model was used for statistical analysis ($n = 8$), with the level of significance set at $p^* < 0.05$ and $p^{**} < 0.01$.

spatiotemporal coupling with the SD-related peak of $[K^+]_e$. More specifically, the onset of vasoconstriction was essentially synchronous with the peak APG-2 fluorescence corresponding to the invading $[K^+]_e$ wave (Fig. 4A–C).

The electrophysiology series of experiments allowed the quantitative assessment of the relationship between $[K^+]_e$ and the early hypoperfusion element of the CBF response to SD. Although results obtained from a number of experiments support the observations presented below, a representative experiment shown in Fig. 5 has been selected to demonstrate the strong link between these variables. This particular experiment was found ideal because of the following favorable conditions: (i) SD events could be studied in the face of baseline $[K^+]_e$ progressively increasing over the experiment from 2.86 to 18.08 mM (Fig. 5C), in the otherwise intact cortex (i.e. no vessel occlusion was imposed). This $[K^+]_e$ gradient departs from the physiological resting state and reaches levels typical of the injured cortex (Hansen and Zeuthen, 1981), but remains within the vasodilator range throughout. This approach was expected to reveal the impact of increasing $[K^+]_e$ on the kinetics of subsequent SDs, independent of any initial limitation of oxygen or glucose availability, and irrespective of any other complex biochemical cascade of events that may take place during an ischemic insult; (ii) The constant arrangement of the potassium-sensitive microelectrode and the laser Doppler probe allowed the monitoring of the same cortical region by each modality from SD to SD, therefore, the evaluation of any change in synchronicity between the $[K^+]_e$ shift and the CBF response to SD could be attained; (iii) A high enough number of rSDs were successfully recorded and quantitated to serve statistical analysis of correlation ($n = 8$).

Correlation analysis confirmed the anticipated lack of interaction between increasing baseline $[K^+]_e$ and resting CBF over the potassium gradient examined ($r = -0.171$, $p = .342$). On the other hand, rising baseline $[K^+]_e$ predicted longer-lasting $[K^+]_e$ shift with rSDs ($r = 0.821$, $p = .006^{**}$) (Fig. $5D_1$), but had no significant impact on the absolute peak of $[K^+]_e$ ($r = 0.580$, $p = .132$) similar to previous observations in brain slices (Dreier et al., 2001). In turn, longer $[K^+]_e$ shift with rSDs was coincident with more prominent early hypoperfusion, characterized by lower CBF minimum reached ($r = -0.842$, $p = .004^{**}$) (Fig. $5D_2$), and greater area under the curve (AUC) ($r = 0.791$, $p = .010^{**}$) (Fig. $5D_3$) similar to previous observations in rats (Dreier et al., 2000). In contrast, the magnitude of hypoperfusion appeared unrelated to the absolute amplitude of the $[K^+]_e$ shift (correlation with CBF minimum: $r = -0.147$, $p = .364$; correlation with AUC of hypoperfusion: $r = 0.282$, $p = .249$).

3.4. Contribution of large-conductance Ca^{2+}-activated K^+ channels or L-type voltage-gated Ca^{2+} channels to potassium-related vasoconstriction in response to SD

The evaluation of pharmacological data focused on the early hypoperfusion element of the CBF response to SD. Only rSD events were considered for the assessment of drug effect, because each pharmacology experiment started with a control phase (i.e. SD1 was triggered before drug application). In order to appreciate the anticipated inhibitory drug effect on the magnitude of hypoperfusion, the control condition was required to produce a sizeable drop of CBF. As shown above, increasing baseline $[K^+]_e$ prior to an SD event predicted greater SD-associated hypoperfusion to follow (Fig. $5D_{1-3}$). Taking these points into consideration, the analysis was conducted on rSDs, which were preceded by a baseline $[K^+]_e$ higher than 10 mM. Following the same reasoning, baseline $[K^+]_e$ prior to rSDs was required to be similar across experimental groups, for the comparison of pharmacological treatments to be meaningful. Indeed, $[K^+]_e$ varied within an overlapping range for all three conditions (16.5 ± 3.6 vs. 17.0 ± 3.2 vs. 14.9 ± 3.1 mM, nimodipine vs. paxilline vs. control; one-way ANOVA:

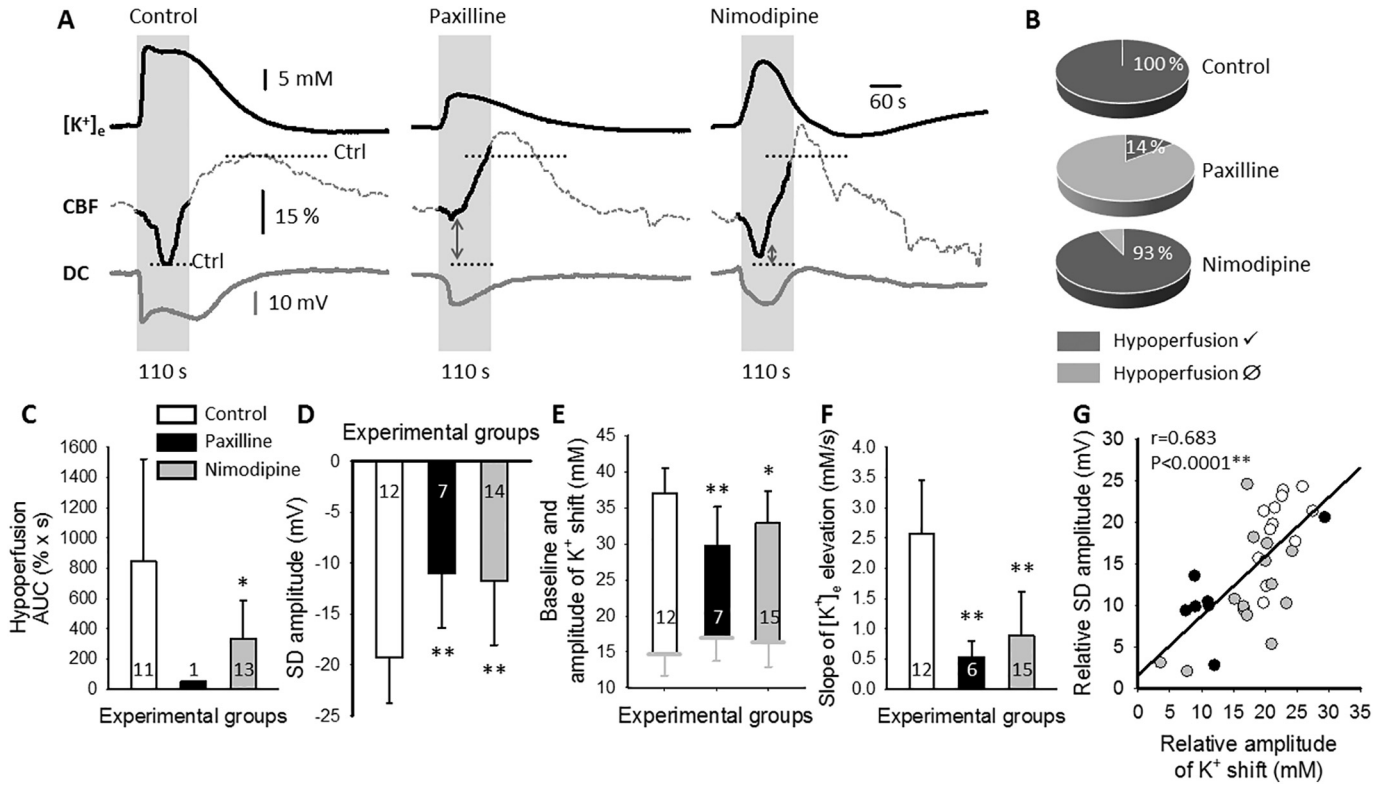

Fig. 6. Pharmacological inhibition of large-conductance Ca^{2+}-activated K^+ (BK) channels by paxilline, and L-type voltage-sensitive Ca^{2+} channels (VGCC) by nimodipine. A, Representative traces demonstrate the extracellular shift in K^+ concentration ($[K^+]_e$; black traces), the direct current (DC) potential signature of spreading depolarization (SD; gray traces), and the corresponding cerebral blood flow (CBF) response (dashed traces) in a control experiment (left), a paxilline-treated preparation (middle), and in case of incubation with nimodipine (right). Horizontal gray dotted lines indicate CBF minimum and CBF maximum in the control experiment, to appreciate changes in the paxilline and nimodipine conditions with respect to control. The gray shaded time segment of the control recording covers the duration of vasoconstriction, and is used as reference in the paxilline and nimodipine experiment. Note that after paxilline or nimodipine treatment, vasodilation already evolves during this time segment of the SD event. B, Pie charts demonstrate the share of SD-coupled CBF responses displaying the first, hypoperfusion element. All SD events analyzed were taken as 100%. Dark gray color indicates CBF responses including early transient hypoperfusion; light gray color stands for CBF responses devoid of the element of early hypoperfusion. C, Both paxilline and nimodipine decreased the area under the curve (AUC) relevant for early hypoperfusion (one-way ANOVA: f = 3.802, p = .038*). For paxilline, early hypoperfusion evolved only in 1 out of 7 SDs. D, Both paxilline and nimodipine treatment reduced the amplitude of the SD-related, negative DC shift (one-way ANOVA: f = 7.683, p = .003**). E, The level of extracellular K^+ prior to SD initiation was similar over the experimental groups (gray line at the base of the bars, and corresponding error bar; one-way ANOVA: f = 1.175, p = .322); paxilline and nimodipine treatment reduced the relative amplitude of the K^+ shift (one-way ANOVA: f = 6.702, p = .004**). F, The rate of the K^+ shift was slower for both the paxilline and nimodipine treated groups (one-way ANOVA: f = 22.791, p < .0001**). For all bar charts, data are given as mean ± stdev; n = 25/33/34/33. Sample size (i.e. number of SD events analyzed) is indicated in each bar. One-way analysis of variance (ANOVA) followed by a Fisher post hoc test was used for statistical analysis. The level of significance is given as p* < 0.05 and p** < 0.01 vs. control. G, The relative amplitude of the K^+ shift with SD shows a positive correlation with the relative amplitude of SD as indicated by the transient, negative shift of the DC potential. A one-tailed Pearson correlation paradigm was used for statistical analysis of the data; n = 33, r = 0.683, p < .0001.

f = 1.175, p < .322; Fig. 6E).

Both paxilline and nimodipine treatment exerted a substantial impact on the CBF response to rSDs under these carefully selected conditions, by impeding the element of initial hypoperfusion and augmenting subsequent peak hyperemia of the CBF response (Fig. 6A). Paxilline, in particular, completely diminished rSD-related hypoperfusion in 6 of 7 cases (Fig. 6B). Nimodipine proved to be less potent; nevertheless, it reduced the magnitude of hypoperfusion (i.e. area under the curve) to the half of the control value (Fig. 6C). Further, paxilline and nimodipine reduced the amplitude of the DC shift with rSDs equally (11.8 ± 6.2 vs. 11.00 ± 5.3 vs. 19.3 ± 4.5 mV, nimodipine vs. paxilline vs. control; Fig. 6D). Finally, both drugs hampered the extracellular accumulation of K^+ with rSDs, which was reflected by the smaller relative amplitude (16.4 ± 6.5 vs. 12.7 ± 7.5 vs. 22.2 ± 2.7 mM, nimodipine vs. paxilline vs. control) and absolute amplitude (32.9 ± 4.4 vs. 29.7 ± 5.4 vs. 37.0 ± 3.5 mM, nimodipine vs. paxilline vs. control; Fig. 6E), and slower rate of rSD-related K^+ surge (i.e. slope; 0.89 ± 0.72 vs. 0.54 ± 0.27 vs. 2.57 ± 0.89 mM/s, nimodipine vs. paxilline vs. control; Fig. 6F). The reduction of the DC amplitude by the treatments appeared to be coincident with the smaller K^+ shift of SD, as indicated by the strong positive correlation between the two variables (Fig. 6G).

In experiments involving neocortical brain slices, the dose of paxilline that delivered consistent and reliable results was found to be 500 nM (data not shown), corresponding to the dose applied in vivo. Our in vitro model system confirmed the in vivo results, in that paxilline significantly reduced the amplitude of the DC shift indicative of rSDs, with respect to SD1 triggered in the same slice under aCSF (−9.1 ± 5.3 vs. -15.7 ± 6.6 mV), and with respect to rSDs triggered in other slices under aCSF (−9.1 ± 5.3 vs. -17.2 ± 5.5 mV) (Fig. 7). In control experiments (i.e. perfused with aCSF throughout the experimental protocol), rSD amplitude fell in the same range as SD1 amplitude (17.2 ± 5.5 vs, 15.3 ± 5.3 mV) (Fig. 7).

4. Discussion

In support of the working hypothesis that a surge of $[K^+]_e$ directly mediates vasoconstriction in response to SD in the cerebral cortex, we

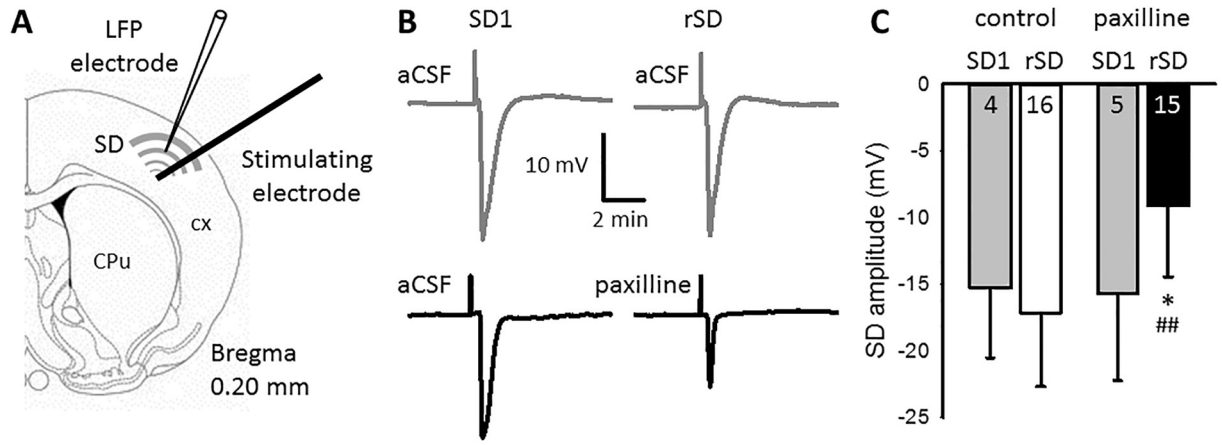

Fig. 7. Pharmacological inhibition of large-conductance Ca^{2+}-activated K^+ (BK) channels by paxilline in acute, live, neocortical brain slices. A, Schematic representation of the preparation used for the recording of local field potential (LFP) that was filtered in direct current (DC) mode. B, Representative traces demonstrate that the amplitude of the negative DC potential shift indicative of spreading depolarization (SD) remains constant under artificial cerebrospinal fluid (aCSF) incubation (gray), but becomes significantly smaller at the presence of 500 nM paxilline (black). SD pairs were taken from representative brain slice preparations. Recurrent SDs (rSDs) shown are the third or fourth SD in a train, elicited 50 min after triggering the respective SD1. C, The amplitude of the negative DC potential shift indicative of SD. Note that in both conditions (i.e. control and 500 nM paxilline), SD1 was triggered under aCSF incubation, and paxilline in the treated group was washed on the slice 8 min prior to initiating rSDs. Data are given as mean ± stdev. Sample size (i.e. number of SD events analyzed) is indicated in each bar. One-way analysis of variance (ANOVA) followed by a Fisher post hoc test was used for statistical analysis. The level of significance is given as $p^* < 0.05$ vs. respective SD1, and $p^{\#\#} < 0.01$ vs. control rSD. Abbreviations: CPu: caudate putamen, cx, cerebral cortex.

implemented a two-photon microscopy approach to visualize the spatio-temporal relationship between $[K^+]_e$ variations and vascular tone. This goal was achieved successfully by the in vivo application of APG-2, a fluorescent indicator of extracellular K^+, in combination with loading the cerebral vasculature with rhodamine dextran. Taken together, this is a pioneering report to show that K^+ imaging with APG-2 can be implemented in a two-photon microscopic setting in anesthetized mice, and is suitable for the detailed assessment of the coupling between $[K^+]_e$ variations and vascular tone.

We present here the original finding that the narrowing of cerebral arterioles – both pial and cortical penetrating arterioles – is spatio-temporally coupled with the sharp increase of $[K^+]_e$ with SD. Moreover, the reduced arteriolar diameter in response to SD must be the result of active vasoconstriction, rather than a potential compression of vessels caused by SD-related swelling of neurons or dendritic beading (Takano et al., 2007; Risher et al., 2010; Zhou et al., 2010), because venules in our preparations maintained unchanging lumen diameter with the passage of each SD.

Pathophysiological events such as ischemic injury first give rise to a moderate elevation of $[K^+]_e$, succeeded by spontaneous, recurrent SDs commencing minutes later (Hansen, 1977; Hansen and Zeuthen, 1981). Typically, the onset of ischemia is followed by a slow rise of $[K^+]_e$ from 3 to 10 mM (Hansen, 1977; Hansen and Zeuthen, 1981), a condition thought to favor the generation of SD. Here we created progressively increasing $[K^+]_e$ in the absence of ischemia to examine how pathophysiological tissue $[K^+]_e$ levels alone relate to the characteristic features of upcoming SD events. Our results demonstrate that increasingly higher $[K^+]_e$ in the cortical volume to be invaded by SD predicts proportionally longer duration of the K^+ shift as SD arrives (Fig. $5D_1$), which confirms previous results in brain slices (Dreier et al., 2001). In other words, the recovery from the K^+ shift with SD is hampered by elevated baseline $[K^+]_e$. This may result from downregulation of α_2 Na^+/K^+-ATPase (Dreier et al., 2001; Major et al., 2017), which in turn impairs the functionality of astrocytes. Thus, in adult somatosensory cortex of rats, the α_2 isoform almost completely co-localizes with the astrocytic glutamate transporters GLAST and GLT1 (EAAT1, EAAT2). Analysis at the ultrastructural level showed that this complex occurs preferentially in astrocytic processes around asymmetric glutamatergic synaptic junctions, but not around GABAergic terminals (Cholet et al., 2002). Insufficient buildup of Na^+ and K^+ gradients in this subcellular microdomain is assumed to decelerate glutamate reuptake, thereby increasing glutamate in the synaptic cleft and delaying neuronal recovery from SD (Moskowitz et al., 2004). As elongated SD duration – corresponding to K^+ shift duration – has been recognized to facilitate the conversion of tissue at risk to infarction during ischemia (Dreier, 2011; Hartings et al., 2017), the data suggest that baseline $[K^+]_e$, prior to and in between recurrent SD events, is a predictive indicator of, and plays a crucial role in ischemic lesion progression.

The early hypoperfusion element of the CBF response to SD has been identified to escalate in the ischemic cortex, to put the survival of metabolically compromised tissue at risk (Shin et al., 2006; Dreier, 2011; Hoffmann and Ayata, 2013; Bere et al., 2014). The inhibition of nitric oxide synthase in combination with high $[K^+]$ was found to cause the outright reduction of perfusion with the onset of SD, a phenomenon that has become known as spreading ischemia (Dreier et al., 1998; Dreier, 2011). Here we confirm that the SD-related K^+ shift alone correlates positively with the depth and magnitude of the early hypoperfusion element of the CBF response to SD in the non-ischemic cortex (Fig. $5D_2$-3) (Dreier et al., 2000). Thus, K^+ accumulation itself appears as a key mediator to determine the degree of early hypoperfusion with SD, which may also result from decline in α_2 Na^+/K^+-ATPase activity because this enhances Ca^{2+} signaling in astrocytes, vascular myocytes, and pericytes (Major et al., 2017). In support of the above suggestion, and to identify potential vasoconstrictive mechanisms downstream to tissue $[K^+]_e$ elevation (Fig. 1), we manipulated the SD-related vasoconstriction by BK channel or L-type VGCC inhibition in the cerebrovascular domain. The selection of pharmacological agents relied on the following grounds. Paxilline given at 1–2 μM concentration successfully inhibited arteriolar dilation evoked by neuronal activation in brain slices, and functional hyperemia in response to whisker-stimulation (Girouard et al., 2010; Koide et al., 2012; Kim et al., 2015). These studies concluded that endfeet BK channels were essential in the regulation of vascular tone during neurovascular coupling. Moreover, the intravenous administration of nimodipine was found to alleviate spreading ischemia with SD under elevated baseline $[K^+]_e$ combined with NO deprivation (Dreier et al., 1998; Dreier et al., 2002). Accordingly, nimodipine also potently antagonized the vasoconstriction imposed by high perivascular $[K^+]_e$ in the isolated middle cerebral artery of rats (Windmüller et al., 2005). With these encouraging evidence in mind, we set out to apply paxilline or nimodipine on the brain surface

of anesthetized mice to evaluate their impact on the SD-coupled initial hypoperfusion under elevated baseline $[K^+]_e$.

Paxilline used here at 500 nM concentration (i.e. half of the lowest concentration reported earlier) exhibited a profound inhibitory effect, by virtually abolishing the early hypoperfusion element of the CBF response to SD (Fig. 6B). Nimodipine, though less potent, also reduced the size of early hypoperfusion remarkably (Fig. 6C). Hence, both pharmacological interventions confirmed the working hypothesis (Fig. 1), and proved the involvement of BK channels and L-type VGCC in the mediation of vasoconstriction in response to SD under elevated baseline $[K^+]_e$. It is noteworthy that paxilline was previously shown to inhibit vasodilation to moderate $[K^+]$ elevation (< 10 mM) (Girouard et al., 2010), while the data gathered here bring new evidence by demonstrating that paxilline blocks vasoconstriction produced by $[K^+]_e$ above 20 mM. As previously discussed (Dreier et al., 1998), the antagonistic effect of nimodipine against the SD-induced vasoconstriction is in agreement with the clinical observation that nimodipine decreased the risk of poor outcome in patients with aSAH by 42% (Tettenborn and Dycka, 1990). Notably, this effect resulted from the reduction in occurrence and severity of delayed cerebral ischemia but not from the reduction of angiographically visible vasospasm (Allen et al., 1983; Espinosa et al., 1984; Petruk et al., 1988).

Whether the drug effects were achieved by the selective targeting of the cerebrovascular domain remains uncertain, because both paxilline and nimodipine reduced the amplitude of SD (Fig. 6D; Fig. 7), and curtailed the evolution of the K^+ shift with SD (Fig. 6E–F). The reduction of SD amplitude is suggested to be directly linked to the treatment-related, decreasing amplitude of the K^+ shift with SD (Fig. 6G) (Hansen and Zeuthen, 1981). The observations with paxilline raise the innovative concept that K^+ efflux during the depolarization phase of SD should manifest through BK channels to a significant degree. Neuronal whole cell patch clamp studies previously provided evidence that the ion dislocations at the rise of SD represent non-selective $Na^+(Ca^{2+})/K^+$ conductances, which implies massive K^+ efflux involving various K^+ channels (Czéh et al., 1992, 1993). Even though neither tetraethylammonium, a drug that targets inward rectifying and delayed outward rectifying K^+ channels (Cook, 1990), nor 4-aminopyridine, a blocker of inward rectifier and A-type K^+ channels (Aitken et al., 1991; Somjen, 2001), were sufficient to fully block SD, they unmasked some contribution of these channels. For example, tetraethylammonium reduced the efflux of K^+. Further, K^+ may leave the cells during SD via ATP-sensitive K^+ channels under metabolic stress (Somjen, 2001). While these non-selective $Na^+(Ca^{2+})/K^+$ conductances probably lead the depolarization, the notable, selective, possibly secondary contribution of BK channels to the SD-related rise of $[K^+]_e$ is first shown here. Nevertheless, the action of paxilline on SD in our experiments was not expected, because concentrations as high as 1 μM had been reported to be selective for astrocytic endfeet, leaving neuronal BK channels unaffected (Girouard et al., 2010). If the 500 nM concentration we used was truly selective for astrocytes, astrocytic BK channels located elsewhere than at the perivascular endfeet must have significantly contributed to the $[K^+]_e$ surge with SD. However, it cannot be excluded that paxilline may have also blocked neuronal BK channels abundant on soma and dendrites, which have been known to adjust neuronal excitability (Latorre et al., 1989; Faber and Sah, 2003), and have been implicated in the reduced susceptibility of the nervous tissue to SD under hypoxia (Hepp et al., 2005). Moreover, blockade of neuronal BK channels with systemic paxilline administration (2.2 μg/kg body weigh) was shown to effectively prevent experimentally induced seizure activity (Sheehan et al., 2009), a pathophysiological phenomenon that shares several mechanisms with SD and can occur together with SD in the acutely injured brain (Fabricius et al., 2008; Dreier et al., 2012). Theoretically, paxilline could have blocked the initial hypoperfusion to SD in our experiments either indirectly, by reducing $[K^+]_e$, or directly, acting on endfeet BK channels. However, because paxilline did not reduce $[K^+]_e$ below the vasoconstrictive threshold (peak amplitude after treatment was 29.7 ± 5.4 mM; Fig. 6E), but abolished SD-induced hypoperfusion almost entirely (Fig. 6B), it is more likely that the inhibition of vasoconstriction was mostly achieved through inhibition of BK channels at the perivascular endfeet.

Nimodipine also altered SD evolution markedly. In addition to VSMC, neurons also express L-type VGCCs, which have been implicated in the modification of neuronal excitability (Moyer Jr et al., 1992), and are a well-known target of neuroprotection to counteract neuronal Ca^{2+} overload in ischemic brain injury (Scriabine et al., 1989; Rami and Krieglstein, 1994). Nimodipine previously inhibited moderately the frequency, latency and amplitude of recurrent SDs triggered with KCl in the rat cerebral cortex at a concentration identical to that used here (Richter et al., 2002). We found, however, that nimodipine considerably reduced the rate and, to a smaller degree, the peak amplitude of the K^+ shift with SD (Fig. 6E–F). In support of our data, nimodipine was found to block 50% of both calcium-dependent and voltage-dependent K^+ currents, recorded in a whole cell patch clamp configuration during action potential firing of cultured rat hippocampal neurons (Caro et al., 2011). In addition, L-type VGCCs were demonstrated to gate BK channels in cortical pyramidal neurons (Contet et al., 2016). It seems, therefore, likely, that in addition to blocking L-type VGCCs on vascular VSMC, nimodipine alleviated the early hypoperfusion element of the CBF response to SD also by slowing outward K^+ currents, thereby weakening K^+-mediated vasoconstriction.

Overall, the data gathered here are highly relevant and translate to neurological disease states (i.e. subarachnoid hemorrhage, ischemic stroke and traumatic brain injury), in which SDs reoccur from minutes to weeks after the primary insult, and contribute to lesion progression by the coupled hypoemic flow transients (Dreier, 2011; Dreier et al., 2017; Hartings et al., 2017). Importantly, high concentration potassium in the nervous tissue emerges as a major cause of SD-related early vasoconstriction. Finally, BK channels – whether at the astrocytic endfeet or on neurons – play a significant role in SD evolution, and the regulation of the associated, early-onset vasoconstriction.

Acknowledgments

This work was supported by grants from the National Research, Development and Innovation Office of Hungary (Grant No. K111923, K120358 and K116158); the Bolyai János Research Scholarship of the Hungarian Academy of Sciences (BO/00023/17/8 to AEF); the Szeged Scientists Academy Program of the Foundation for the Future of Biomedical Sciences in Szeged, implemented with the support of the Ministry of Human Capacities of Hungary (No. 34232-3/2016/INTFIN, to RT and ARB); the New National Excellence Program of the Ministry of Human Capacities of Hungary (No. UNKP-17-1-I-SZTE-34 to RT and UNKP-17-2-I-SZTE-2 to ARB); the Economic Development and Innovation Operational Programme in Hungary co-financed by the European Union and the European Regional Development Fund (No. GINOP-2.3.2-15-2016-00048, GINOP-2.3.2-15-2016-0020, GINOP-2.3.2-15-2016-0030, GINOP-2.3.2-15-2016-0034); PN-III-P4-ID-PCE-2016-0408 (188/2017); the EU-funded Hungarian grant No. EFOP-3.6.1-16- 2016-00008, the Deutsche Forschungsgemeinschaft (DFG DR 323/5-1), and the Bundesministerium für Bildung und Forschung (BMBF CSB 01 EO 0801).

Author contributions

Á. Menyhárt and E. Farkas designed research; Á. Menyhárt, A.E. Farkas, D.P. Varga, R. Frank, R. Tóth, A.R. Bálint and P. Makra analyzed data; Á. Menyhárt, A.E. Farkas, D.P. Varga and R. Frank performed research; E. Farkas, Á. Menyhárt; A.E. Farkas, J.P. Dreier, F. Bari and I.A. Krizbai wrote the paper; I.A. Krizbai, F. Bari and E. Farkas contributed analytic tools.

Conflicts of interest

The authors declare no conflict of interest.

References

Aitken, P.G., Jing, J., Young, J., Somjen, G.G., 1991 Feb 8. Ion channel involvement in hypoxia-induced spreading depression in hippocampal slices. Brain Res. 541 (1), 7–11.

Alborch, E., Salom, J.B., Torregrosa, G., 1995. Calcium channels in cerebral arteries. Pharmacol. Ther. 68 (1), 1–34.

Allen, G.S., Ahn, H.S., Preziosi, T.J., Battye, R., Boone, S.C., Boone, S.C., Chou, S.N., Kelly, D.L., Weir, B.K., Crabbe, R.A., Lavik, P.J., Rosenbloom, S.B., Dorsey, F.C., Ingram, C.R., Mellits, D.E., Bertsch, L.A., Boisvert, D.P., Hundley, M.B., Johnson, R.K., Strom, J.A., Transou, C.R., 1983 Mar 17. Cerebral arterial spasm–a controlled trial of nimodipine in patients with subarachnoid hemorrhage. N. Engl. J. Med. 308 (11), 619–624.

Attwell, D., Buchan, A.M., Charpak, S., Lauritzen, M., Macvicar, B.A., Newman, E.A., 2010 Nov 11. Glial and neuronal control of brain blood flow. Nature 468 (7321), 232–243. https://doi.org/10.1038/nature09613.

Ayata, C., Lauritzen, M., 2015 Jul. Spreading depression, spreading depolarizations, and the cerebral vasculature. Physiol. Rev. 95 (3), 953–993. https://doi.org/10.1152/physrev.00027.2014.

Bazzigaluppi, P., Dufour, S., Carlen, P.L., 2015. Wide field fluorescent imaging of extracellular spatiotemporal potassium dynamics in vivo. Neuroimage. 104, 110–116. https://doi.org/10.1016/j.neuroimage.2014.10.012. Jan 1.

Bere, Z., Obrenovitch, T.P., Kozák, G., Bari, F., Farkas, E., 2014 Oct. Imaging reveals the focal area of spreading depolarizations and a variety of hemodynamic responses in a rat microembolic stroke model. J. Cereb. Blood Flow Metab. 34 (10), 1695–1705. https://doi.org/10.1038/jcbfm.2014.136.

Caro, A., Tarabova, B., Rojo-Ruiz, J., Lacinova, L., 2011. Nimodipine inhibits AP firing in cultured hippocampal neurons predominantly due to block of voltage-dependent potassium channels. Gen. Physiol. Biophys. 30https://doi.org/10.4149/gpb_2011_SI1_44. Spec No:S44-53.

Cholet, N., Pellerin, L., Magistretti, P.J., Hamel, E., 2002 May. Similar perisynaptic glial localization for the Na+,K+-ATPase alpha 2 subunit and the glutamate transporters GLAST and GLT-1 in the rat somatosensory cortex. Cereb. Cortex 12 (5), 515–525.

Contet, C., Goulding, S.P., Kuljis, D.A., Barth, A.L., 2016. BK channels in the central nervous system. Int. Rev. Neurobiol. 128, 281–342. https://doi.org/10.1016/bs.irn.2016.04.001.

Cook, N.S., 1990. Potassium Channels: Structure, Classification, Functional and Therapeutic Potential. Harwood Halsted Press, Great Britain.

Czéh, G., Aitken, P.G., Somjen, G.G., 1992 Feb. Hole-cell membrane current and membrane resistance during hypoxic spreading depression. Neuroreport 3 (2), 197–200.

Czéh, G., Aitken, P.G., Somjen, G.G., 1993 Dec 31. Membrane currents in CA1 pyramidal cells during spreading depression (SD) and SD-like hypoxic depolarization. Brain Res. 632 (1–2), 195–208.

Dreier, J.P., 2011 Apr. The role of spreading depression, spreading depolarization and spreading ischemia in neurological disease. Nat. Med. 17 (4), 439–447. https://doi.org/10.1038/nm.2333.

Dreier, J.P., Reiffurth, C., 2015 May 20. The stroke-migraine depolarization continuum. Neuron 86 (4), 902–922. https://doi.org/10.1016/j.neuron.2015.04.004.

Dreier, J.P., Körner, K., Ebert, N., Görner, A., Rubin, I., Back, T., Lindauer, U., Wolf, T., Villringer, A., Einhäupl, K.M., Lauritzen, M., Dirnagl, U., 1998 Sep. Nitric oxide scavenging by hemoglobin or nitric oxide synthase inhibition by N-nitro-L-arginine induces cortical spreading ischemia when K+ is increased in the subarachnoid space. J. Cereb. Blood Flow Metab. 18 (9), 978–990.

Dreier, J.P., Ebert, N., Priller, J., Megow, D., Lindauer, U., Klee, R., Reuter, U., Imai, Y., Einhäupl, K.M., Victorov, I., Dirnagl, U., 2000 Oct. Products of hemolysis in the subarachnoid space inducing spreading ischemia in the cortex and focal necrosis in rats: a model for delayed ischemic neurological deficits after subarachnoid hemorrhage? J. Neurosurg. 93 (4), 658–666.

Dreier, J.P., Petzold, G., Tille, K., Lindauer, U., Arnold, G., Heinemann, U., Einhäupl, K.M., Dirnagl, U., 2001 Mar 1. Ischaemia triggered by spreading neuronal activation is inhibited by vasodilators in rats. J. Physiol. 531 (Pt 2), 515–526.

Dreier, J.P., Windmüller, O., Petzold, G., Lindauer, U., Einhäupl, K.M., Dirnagl, U., 2002 Dec. Ischemia triggered by red blood cell products in the subarachnoid space is inhibited by nimodipine administration or moderate volume expansion/hemodilution in rats. Neurosurgery 51 (6), 1457–1465 (discussion 1465-7).

Dreier, J.P., Major, S., Manning, A., Woitzik, J., Drenckhahn, C., Steinbrink, J., Tolias, C., Oliveira-Ferreira, A.I., Fabricius, M., Hartings, J.A., Vajkoczy, P., Lauritzen, M., Dirnagl, U., Bohner, G., 2009 Jul. Strong AJ; COSBID study group. Cortical spreading ischaemia is a novel process involved in ischaemic damage in patients with aneurysmal subarachnoid haemorrhage. Brain 132 (Pt 7), 1866–1881. https://doi.org/10.1093/brain/awp102.

Dreier, J.P., Major, S., Pannek, H.W., Woitzik, J., Scheel, M., Wiesenthal, D., Martus, P., Winkler, M.K., Hartings, J.A., Fabricius, M., Speckmann, E.J., 2012 Jan. Gorji a; COSBID study group. Spreading convulsions, spreading depolarization and epileptogenesis in human cerebral cortex. Brain 135 (Pt 1), 259–275. https://doi.org/10.1093/brain/awr303.

Dreier, J.P., Fabricius, M., Ayata, C., Sakowitz, O.W., William Shuttleworth, C., Dohmen, C., Graf, R., Vajkoczy, P., Helbok, R., Suzuki, M., Schiefecker, A.J., Major, S., Winkler, M.K., Kang, E.J., Milakara, D., Oliveira-Ferreira, A.I., Reiffurth, C., Revankar, G.S., Sugimoto, K., Dengler, N.F., Hecht, N., Foreman, B., Feyen, B., Kondziella, D., Friberg, C.K., Piilgaard, H., Rosenthal, E.S., Westover, M.B., Maslarova, A., Santos, E., Hertle, D., Sánchez-Porras, R., Jewell, S.L., Balança, B., Platz, J., Hinzman, J.M., Lückl, J., Schoknecht, K., Schöll, M., Drenckhahn, C., Feuerstein, D., Eriksen, N., Horst, V., Bretz, J.S., Jahnke, P., Scheel, M., Bohner, G., Rostrup, E., Pakkenberg, B., Heinemann, U., Claassen, J., Carlson, A.P., Kowoll, C.M., Lublinsky, S., Chassidim, Y., Shelef, I., Friedman, A., Brinker, G., Reiner, M., Kirov, S.A., Andrew, R.D., Farkas, E., Güresir, E., Vatter, H., Chung, L.S., Brennan, K.C., Lieutaud, T., Marinesco, S., Maas, A.I., Sahuquillo, J., Dahlem, M.A., Richter, F., Herreras, O., Boutelle, M.G., Okonkwo, D.O., Bullock, M.R., Witte, O.W., Martus, P., van den Maagdenberg, A.M., Ferrari, M.D., Dijkhuizen, R.M., Shutter, L.A., Andaluz, N., Schulte, A.P., MacVicar, B., Watanabe, T., Woitzik, J., Lauritzen, M., Strong, A.J., Hartings, J.A., 2017 May. Recording, analysis, and interpretation of spreading depolarizations in neurointensive care: Review and recommendations of the COSBID research group. J. Cereb. Blood Flow Metab. 37 (5), 1595–1625. https://doi.org/10.1177/0271678X16654496.

Dreier, J.P., Major, S., Foreman, B., Winkler, M.K.L., Kang, E.J., Milakara, D., Lemale, C.L., Dinapoli, V., Hinzman, J.M., Woitzik, J., Andaluz, N., Carlson, A., Hartings, J.A., 2018 Feb. Erminal spreading depolarization and electrical silence in death of human cerebral cortex. Ann. Neurol. 83 (2), 295–310. https://doi.org/10.1002/ana.25147.

Espinosa, F., Weir, B., Overton, T., Castor, W., Grace, M., Boisvert, D., 1984 Jun. A randomized placebo-controlled double-blind trial of nimodipine after SAH in monkeys. Part 1: clinical and radiological findings. J. Neurosurg. 60 (6), 1167–1175.

Faber, E.S., Sah, P., 2003 Jun. Calcium-activated potassium channels: multiple contributions to neuronal function. Neuroscientist 9 (3), 181–194.

Fabricius, M., Fuhr, S., Willumsen, L., Dreier, J.P., Bhatia, R., Boutelle, M.G., Hartings, J.A., Bullock, R., Strong, A.J., Lauritzen, M., 2008 Sep. Association of seizures with cortical spreading depression and peri-infarct depolarisations in the acutely injured human brain. Clin. Neurophysiol. 119 (9), 1973–1984. https://doi.org/10.1016/j.clinph.2008.05.025.

Farkas, E., Bari, F., Obrenovitch, T.P., 2010 Jun. Multi-modal imaging of anoxic depolarization and hemodynamic changes induced by cardiac arrest in the rat cerebral cortex. NeuroImage 51 (2), 734–742. https://doi.org/10.1016/j.neuroimage.2010.02.055.

Filosa, J.A., Bonev, A.D., Straub, S.V., Meredith, A.L., Wilkerson, M.K., Aldrich, R.W., Nelson, M.T., 2006 Nov. Local potassium signaling couples neuronal activity to vasodilation in the brain. Nat. Neurosci. 9 (11), 1397–1403.

Girouard, H., Bonev, A.D., Hannah, R.M., Meredith, A., Aldrich, R.W., Nelson, M.T., 2010 Feb 23. Astrocytic endfoot Ca2+ and BK channels determine both arteriolar dilation and constriction. Proc. Natl. Acad. Sci. U. S. A. 107 (8), 3811–3816. https://doi.org/10.1073/pnas.0914722107.

Golding, E.M., Steenberg, M.L., Johnson, T.D., Bryan Jr., R.M., 2000 Oct 13. The effects of potassium on the rat middle cerebral artery. Brain Res. 880 (1–2), 159–166.

Hansen, A.J., 1977 Apr. Extracellular potassium concentration in juvenile and adult rat brain cortex during anoxia. Acta Physiol. Scand. 99 (4), 412–420.

Hansen, A.J., Zeuthen, T., 1981 Dec. Extracellular ion concentrations during spreading depression and ischemia in the rat brain cortex. Acta Physiol. Scand. 113 (4), 437–445.

Hartings, J.A., Shuttleworth, C.W., Kirov, S.A., Ayata, C., Hinzman, J.M., Foreman, B., Andrew, R.D., Boutelle, M.G., Brennan, K.C., Carlson, A.P., Dahlem, M.A., Drenckhahn, C., Dohmen, C., Fabricius, M., Farkas, E., Feuerstein, D., Graf, R., Helbok, R., Lauritzen, M., Major, S., Oliveira-Ferreira, A.I., Richter, F., Rosenthal, E.S., Sakowitz, O.W., Sánchez-Porras, R., Santos, E., Schöll, M., Strong, A.J., Urbach, A., Westover, M.B., Winkler, M.K., Witte, O.W., Woitzik, J., Dreier, J.P., 2017 May. The continuum of spreading depolarizations in acute cortical lesion development: Examining Leão's legacy. J. Cereb. Blood Flow Metab. 37 (5), 1571–1594. https://doi.org/10.1177/0271678X16654495.

Hepp, S., Gerich, F.J., Müller, M., 2005 Aug. Sulfhydryl oxidation reduces hippocampal susceptibility to hypoxia-induced spreading depression by activating BK channels. J. Neurophysiol. 94 (2), 1091–1103.

Hertelendy, P., Menyhárt, Á., Makra, P., Süle, Z., Kiss, T., Tóth, G., Iványkovits-Kiss, O., Bari, F., Farkas, E., 2017 May. Advancing age and ischemia elevate the electric threshold to elicit spreading depolarization in the cerebral cortex of young adult rats. J. Cereb. Blood Flow Metab. 37 (5), 1763–1775. https://doi.org/10.1177/0271678X16643735.

Hinzman, J.M., Andaluz, N., Shutter, L.A., Okonkwo, D.O., Pahl, C., Strong, A.J., Dreier, J.P., Hartings, J.A., 2014 Nov. Inverse neurovascular coupling to cortical spreading depolarizations in severe brain trauma. Brain 137 (Pt 11), 2960–2972. https://doi.org/10.1093/brain/awu241.

Hoffmann, U., Ayata, C., 2013. Neurovascular coupling during spreading depolarizations. Acta Neurochir. Suppl. 115, 161–165. https://doi.org/10.1007/978-3-7091-1192-5_31.

Horrigan, F.T., Aldrich, R.W., 2002 Sep. Coupling between voltage sensor activation, Ca2+ binding and channel opening in large conductance (BK) potassium channels. J. Gen. Physiol. 120 (3), 267–305 (Erratum in: J Gen Physiol. 2002 Oct;120(4):599).

Hsu, Y.C., Hsu, C.H., Tseng, W.Y., 2012 Nov 1. A large deformation diffeomorphic metric mapping solution for diffusion spectrum imaging datasets. NeuroImage 63 (2), 818–834. https://doi.org/10.1016/j.neuroimage.2012.07.033.

Kim, K.J., Iddings, J.A., Stern, J.E., Blanco, V.M., Croom, D., Kirov, S.A., Filosa, J.A., 2015 May 27. Astrocyte contributions to flow/pressure-evoked parenchymal arteriole vasoconstriction. J. Neurosci. 35 (21), 8245–8257. https://doi.org/10.1523/JNEUROSCI.4486-14.2015.

Kocsis, K., Frank, R., Szabó, J., Knapp, L., Kis, Z., Farkas, T., Vécsei, L., Toldi, J., 2016 Sep 22. Acetyl-l-carnitine restores synaptic transmission and enhances the inducibility of stable LTP after oxygen-glucose deprivation. Neuroscience 332, 203–211. https://doi.org/10.1016/j.neuroscience.2016.06.046.

Koide, M., Bonev, A.D., Nelson, M.T., Wellman, G.C., 2012 May 22. Inversion of

neurovascular coupling by subarachnoid blood depends on large-conductance Ca2+ −activated K+ (BK) channels. Proc. Natl. Acad. Sci. U. S. A. 109 (21), E1387–E1395. https://doi.org/10.1073/pnas.1121359109.
Kuschinsky, W., Wahl, M., Bosse, O., Thurau, K., 1972 Aug. Perivascular potassium and pH as determinants of local pial arterial diameter in cats. A microapplication study. Circ. Res. 31 (2), 240–247.
Larsen, B.R., MacAulay, N., 2017 Oct. Activity-dependent astrocyte swelling is mediated by pH-regulating mechanisms. Glia 65 (10), 1668–1681. https://doi.org/10.1002/glia.23187.
Latorre, R., Oberhauser, A., Labarca, P., Alvarez, O., 1989. Varieties of calcium-activated potassium channels. Annu. Rev. Physiol. 51, 385–399.
Lauritzen, M., Dreier, J.P., Fabricius, M., Hartings, J.A., Graf, R., Strong, A.J., 2011 Jan. Clinical relevance of cortical spreading depression in neurological disorders: migraine, malignant stroke, subarachnoid and intracranial hemorrhage, and traumatic brain injury. J. Cereb. Blood Flow Metab. 31 (1), 17–35. https://doi.org/10.1038/jcbfm.2010.191.
Li, B., Chen, S., Zeng, S., Luo, Q., Li, P., 2012. Modeling the contributions of Ca2+ flows to spontaneous Ca2+ oscillations and cortical spreading depression-triggered Ca2+ waves in astrocyte networks. PLoS One 7 (10), e48534. https://doi.org/10.1371/journal.pone.0048534.
Major, S., Petzold, G.C., Reiffurth, C., Windmüller, O., Foddis, M., Lindauer, U., Kang, E.J., Dreier, J.P., 2017 May. A role of the sodium pump in spreading ischemia in rats. J. Cereb. Blood Flow Metab. 37 (5), 1687–1705. https://doi.org/10.1177/0271678X16639059.
Moskowitz, M.A., Bolay, H., Dalkara, T., 2004 Feb. Deciphering migraine mechanisms: clues from familial hemiplegic migraine genotypes. Ann. Neurol. 55 (2), 276–280.
Moyer Jr., J.R., Thompson, L.T., Black, J.P., Disterhoft, J.F., 1992 Dec. Nimodipine increases excitability of rabbit CA1 pyramidal neurons in an age- and concentration-dependent manner. J. Neurophysiol. 68 (6), 2100–2109.
Petruk, K.C., West, M., Mohr, G., Weir, B.K., Benoit, B.G., Gentili, F., Disney, L.B., Khan, M.I., Grace, M., Holness, R.O., et al., 1988 Apr. Nimodipine treatment in poor-grade aneurysm patients. Results of a multicenter double-blind placebo-controlled trial. J. Neurosurg. 68 (4), 505–517.
Petzold, G.C., Windmüller, O., Haack, S., Major, S., Buchheim, K., Megow, D., Gabriel, S., Lehmann, T.N., Drenckhahn, C., Peters, O., Meierkord, H., Heinemann, U., Dirnagl, U., Dreier, J.P., 2005 Jun. Increased extracellular K+ concentration reduces the efficacy of N-methyl-D-aspartate receptor antagonists to block spreading depression-like depolarizations and spreading ischemia. Stroke 36 (6), 1270–1277.
Pietrobon, D., Moskowitz, M.A., 2014 Jun. Chaos and commotion in the wake of cortical spreading depression and spreading depolarizations. Nat. Rev. Neurosci. 15 (6), 379–393. https://doi.org/10.1038/nrn3770.
Rami, A., Krieglstein, J., 1994. Neuronal protective effects of calcium antagonists in cerebral ischemia. Life Sci. 55 (25–26), 2105–2113.
Richter, F., Ebersberger, A., Schaible, H.G., 2002 Dec 13. Blockade of voltage-gated calcium channels in rat inhibits repetitive cortical spreading depression. Neurosci. Lett. 334 (2), 123–126.
Risher, W.C., Ard, D., Yuan, J., Kirov, S.A., 2010 Jul 21. Recurrent spontaneous spreading depolarizations facilitate acute dendritic injury in the ischemic penumbra. J. Neurosci. 30 (29), 9859–9868. https://doi.org/10.1523/JNEUROSCI.1917-10.2010.
Schindelin, J., Arganda-Carreras, I., Frise, E., Kaynig, V., Longair, M., Pietzsch, T., Preibisch, S., Rueden, C., Saalfeld, S., Schmid, B., Tinevez, J.Y., White, D.J., Hartenstein, V., Eliceiri, K., Tomancak, P., Cardona, A., 2012 Jun 28. Fiji: an open-source platform for biological-image analysis. Nat. Methods 9 (7), 676–682. https://doi.org/10.1038/nmeth.2019.
Scriabine, A., Schuurman, T., Traber, J., 1989 May. Pharmacological basis for the use of nimodipine in central nervous system disorders. FASEB J. 3 (7), 1799–1806.
Sheehan, J.J., Benedetti, B.L., Barth, A.L., 2009 Apr. Anticonvulsant effects of the BK-channel antagonist paxilline. Epilepsia 50 (4), 711–720. https://doi.org/10.1111/j.1528-1167.2008.01888.x.
Shin, H.K., Dunn, A.K., Jones, P.B., Boas, D.A., Moskowitz, M.A., Ayata, C., 2006 Aug. Vasoconstrictive neurovascular coupling during focal ischemic depolarizations. J. Cereb. Blood Flow Metab. 26 (8), 1018–1030.
Somjen, G.G., 1979. Extracellular potassium in the mammalian central nervous system. Annu. Rev. Physiol. 41, 159–177.
Somjen, G.G., 2001 Jul. Mechanisms of spreading depression and hypoxic spreading depression-like depolarization. Physiol. Rev. 81 (3), 1065–1096.
Takano, T., Tian, G.F., Peng, W., Lou, N., Lovatt, D., Hansen, A.J., Kasischke, K.A., Nedergaard, M., 2007 Jun. Cortical spreading depression causes and coincides with tissue hypoxia. Nat. Neurosci. 10 (6), 754–762.
Tettenborn, D., Dycka, J., 1990 Dec. Prevention and treatment of delayed ischemic dysfunction in patients with aneurysmal subarachnoid hemorrhage. Stroke 21 (12 Suppl), IV85–9.
Viitanen, T., Ruusuvuori, E., Kaila, K., Voipio, J., 2010 May 1. The K+-Cl cotransporter KCC2 promotes GABAergic excitation in the mature rat hippocampus. J. Physiol. 588 (Pt 9), 1527–1540. https://doi.org/10.1113/jphysiol.2009.181826.
Vyskocil, F., Kritz, N., Bures, J., 1972 Apr 14. Potassium-selective microelectrodes used for measuring the extracellular brain potassium during spreading depression and anoxic depolarization in rats. Brain Res. 39 (1), 255–259.
Windmüller, O., Lindauer, U., Foddis, M., Einhäupl, K.M., Dirnagl, U., Heinemann, U., Dreier, J.P., 2005 Sep. Ion changes in spreading ischaemia induce rat middle cerebral artery constriction in the absence of NO. Brain 128 (Pt 9), 2042–2051.
Woitzik, J., Hecht, N., Pinczolits, A., Sandow, N., Major, S., Winkler, M.K., Weber-Carstens, S., Dohmen, C., Graf, R., Strong, A.J., Dreier, J.P., 2013 Mar 19. Vajkoczy P; COSBID study group. Propagation of cortical spreading depolarization in the human cortex after malignant stroke. Neurology 80 (12), 1095–1102. https://doi.org/10.1212/WNL.0b013e3182886932.
Zhou, N., Gordon, G.R., Feighan, D., MacVicar, B.A., 2010 Nov. Transient swelling, acidification, and mitochondrial depolarization occurs in neurons but not astrocytes during spreading depression. Cereb. Cortex 20 (11), 2614–2624. https://doi.org/10.1093/cercor/bhq018.